P1.7   TOTAL LIGHTNING AND RADAR CHARACTERISTICS OF SUPERCELLS:
INSIGHTS ON ELECTRIFICATION AND SEVERE WEATHER FORECASTING

Scott M. Steiger*, Richard E. Orville
Texas A&M University, College Station, Texas

Martin J. Murphy, Nicholas W. S. Demetriades
Vaisala, Inc., Tucson, Arizona

1.   INTRODUCTION

Lightning and radar observations are used to characterize thunderstorms and to warn people of imminent severe weather. Combined, these two data sets form the foundation of short term forecasting of convective weather. Also, relationships between radar and lightning characteristics give insight into how a thunderstorm's dynamics and electrification processes operate. The advent of the WSR-88D nationwide (U. S.) radar system, National Lightning Detection Network (NLDN), and 3-dimensional lightning mapping systems (here we use the Lightning Detection and Ranging Dallas-Fort Worth (LDAR II) network) allows scientists to dissect thunderstorms and develop relationships between observables.

Total (intracloud (IC) and cloud-to-ground (CG)) lightning data has distinct advantages over having CG data alone in that the first lightning discharge in a thunderstorm is typically IC and a high percentage (typically well over 50%) of flashes in a storm are IC. Hence, having both LDAR II and NLDN data give a comprehensive overview of a thunderstorm's electrical development. A key characteristic used in this study is the height of lightning activity and relating this to storm evolution and severity. MacGorman et al. (1981) show that lightning activity tends to concentrate in layers, often in a bimodal height distribution. An experiment conducted by Williams et al. (1985) shows that discharge propagation occurs in regions of maximum space charge density (lightning "seeks out" regions of charge). The above two results suggest that total lightning detection by such instruments as the LDAR II can map out the main charge regions in a thunderstorm.

Supercells are prolific lightning producers, and some studies suggest they may have unique lightning characteristics that may help predict the severe weather that can accompany them. MacGorman et al. (1989) found that the number of strokes to ground increase after the tornadic stage of a storm ends. The ground flash rate was negatively correlated with cyclonic shear. However, there was a strong correlation between IC flash rate and cyclonic shear at 1.5 km altitude. To explain this, MacGorman et al. propose the elevated charge region hypothesis: As a storm's updraft intensifies, the main negative charge region is uplifted and brought closer to the main positive charge region typically located higher in the storm, and IC flashes will become more frequent and CG flash rates will decrease; when the updraft weakens, CG flash rates will increase as the lower negative charge region descends closer to the ground. MacGorman and Nielsen (1991) show the opposite relationship in the "Edmond storm:" as low-level cyclonic shear initially increased, negative CG lightning flash rates also increased. It is clear that robust relationships between storm dynamics, severe weather, and lightning activity are lacking. A major purpose of this study is to better understand how we may use total lightning information in describing storm behavior. A comparison between charge region heights (revealed by lightning mapping), IC/CG rates, and radar characteristics will be shown to test these hypotheses.

A mesoscale convective system (MCS) transgressed the Dallas-Fort Worth area late on 12 October to early 13 October 2001. Embedded in this system were several supercells, a couple of which were intense and produced F2 tornadoes and large hail. This provides an excellent opportunity to compare severe storm reports, radar and lightning data from the NLDN and LDAR II to test the following hypotheses: (1) the peaks in the height distribution of lightning activity detected by LDAR II represent charge regions, (2) there are spatial/temporal signatures in the lightning data that predict severe weather, (3) the elevated charge region hypothesis (MacGorman et al. 1989), and (4) most total lightning activity is concentrated near regions of reflectivity gradient.

_____

* _Corresponding author address:_ Scott M. Steiger, SUNY Oswego, Dept. of Earth Sciences, Oswego, NY 13126; e-mail: steiger@oswego.edu.

2. DATA AND METHODOLOGY

The radar data used in this study were from the Dallas-Fort Worth WSR-88D (KFWS), obtained from the National Climatic Data Center (NCDC). This S-band (10 cm wavelength) Doppler radar has a half-power beamwidth of approximately 0.95°, a gate spacing of 1 km, and can sample reflectivity fields at horizontal distances of 460 km. To initially analyze the collected data, we used the WDSS-II (Warning Decision Support System-Integrated Information) software (Hondl 2003) provided by the National Severe Storms Laboratory (NSSL). This software has algorithms that identify, track (Storm Cell Identification and Tracking (SCIT) algorithm, Johnson et al. 1998), and quantitatively describe the state of storm cells (Hail Detection Algorithm (HDA), Witt et al. 1998, and Mesocyclone Detection Algorithm (MDA), Stumpf et al. 1998). The FWD (Dallas-Fort Worth) sounding was used to obtain temperature level data to import into the HDA. Storm cells, and hence lightning data, will be analyzed only within a range of 30 to 100 km away from the KFWS radar site due to the cone of silence and beam elevation effects (lowest tilt beam is above the freezing level at far ranges, and this causes systematic error in the HDA), and the poor resolution and detection efficiency of the LDAR II instrument beyond 150 km from the network center. Note that the radar is approximately 45 km to the southwest of the LDAR II network center. Radar data was also converted from a polar to a Cartesian grid space using REORDER software (Oye and Case 1995). The horizontal and vertical grid spacings were set at 1.0 and 0.5 km, respectively. In this way, lightning (LDAR II source points, CG flash locations) were overlaid on radar reflectivity values for comparisons between the two data sets.

Cummins et al. (2000) describe three lightning detection technologies and location methods that employ networks of radiation-field sensors. The technologies are segregated by frequency ranges of operation: very low frequency (VLF), low frequency (LF), and very high frequency (VHF). Each has its own advantages. Breakdown and ionization processes (leaders and streamers) emit strongly in the VHF, while high currents which occur in previously ionized channels (CG return strokes) have their most powerful emissions in the LF and VLF ranges. Hence, CG lightning detection utilizes the lower frequency ranges while IC mapping is conducted using the VHF band.

The cloud-to-ground (CG) lightning data used in this study were from the National Lighting Detection Network (NLDN). These data were obtained from Vaisala, Inc., Tucson, AZ. The network consists of 106 sensors across the U. S. (Orville and Huffines 1999). The NLDN was given an upgrade in 1994 (Cummins et al. 1998). This upgrade included a combination of improved accuracy from combined technology (IMPACT) and time-of-arrival (TOA) sensors. The upgrade resulted in improving the median accuracy to 500 m and expected flash detection efficiency to ~85% for events with peak currents above 5 kA. The CG lightning characteristics that were analyzed from these data include: negative and positive flash density, percent positive flashes, median peak current for both polarity flashes, and mean multiplicity for each polarity.

Total lightning flash data over the Dallas-Fort Worth area were from the VHF lightning mapping instrumentation known as the Lightning Detection and Ranging (LDAR II) network operated and maintained by Vaisala, Inc. Because VHF impulses are of short duration and have line-of-sight propagation, they can be modeled as point sources located in three dimensions (thousands of which can comprise a single flash). The LDAR II uses the time-of-arrival (TOA) technique described in Proctor (1971). This network is composed of 7 sensors with 20 to 30 km baselines centered on the Dallas-Fort Worth International Airport (Fig. 1). The regional LDAR II network can accurately map lightning flashes in 3-dimensions within approximately 150 km of the center of the network, degrading in performance with increasing range (Demetriades et al. 2001). The expected lightning *flash* detection efficiency is typically greater than 95% within 30 km (the interior of the network) from the DFW International Airport, and greater than 90% out to a range of 100 km. Expected 3-dimensional location accuracy for individual pulses of radiation is between 100 and 200 m within the interior of the network and better than 2 km to a range of 150 km. LDAR II VHF sources were grouped into flashes according to temporal and spatial restrictions using an IDL (Interactive Data Language) program provided by Dr. Gary Huffines. It is a modified version of an algorithm created by NASA. The constraints used to determine if a source was part of a flash were: a maximum of 3 s for the duration of the flash, maximum time lag of 0.5 s between points in a flash, maximum time delay of 0.03 s between points in a branch and points must be within 5 km
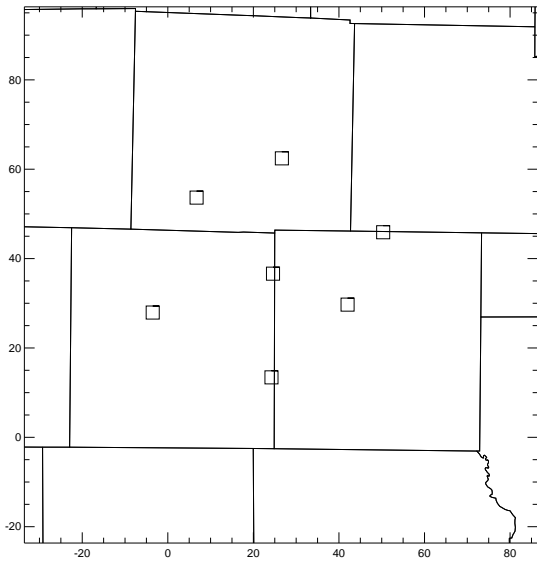
Figure 1. Locations of Dallas-Ft. Worth LDAR II sites (squares). The center site is located at the DFW Airport. The x and y axes are labeled according to distance from the KFWS WSR-88D. County outlines are also shown.

of each other to be considered part of the same flash.

There are a few drawbacks to using a system like the LDAR II for lightning detection. Its limited useful range is one of them, owing to VHF signal attenuation, loss of below-horizon VHF sources (due to line-of-sight propagation), and increasing location errors at far ground ranges (Boccippio et al. 2000). Comparatively few sources are observed from CG leaders because of how IC and CG channels radiate differently. The total source density is thus dominated by the in-cloud portion of total lightning flashes. According to the interpretations by Mazur et al. (1997), continuously propagating positive leaders do not emit sufficiently strong VHF radiation to be detected by LDAR technology, LDAR does not map radiation sources well that are associated with stepped and dart leaders propagating toward the ground, and the LDAR is inadequate to map K changes inside the cloud (K changes, or recoil streamers, are fast current pulses that propagate in a direction opposite to the initial channel development (MacGorman and Rust 1998, p. 92)). The TOA system best locates radiation sources of slow negative breakdown processes at the tip(s) of propagating negative leaders. From these findings, Mazur et al. conclude TOA systems like the LDAR II map best the continuously developing intracloud processes.

To compare the lightning and radar characteristics of storm cells, we examined lightning data (CG and total) within 5, 10, and 20 km of the radar-defined cell or mesocyclone (cell/mesocyclone locations given by WDSS-II). We will show the 10 km results as most lightning from the storms of interest were contained within this distance without contamination from nearby storms. This resulted in cylindrical volumes of total lightning data from LDAR II. The radar and lightning characteristics analyzed included: storm cell maximum reflectivity, maximum reflectivity height, radar top (maximum height of the 30 dBZ contour), severe hail index (SHI), vertically integrated liquid (VIL), low-level mesocyclone diameter, mesocyclone strength index (MSI), lower quartile, median, 95th percentile (lightning-based storm top), and peak height of LDAR II sources, number of modes (peaks) in the height distribution of sources, normalized peak value of sources, half power thickness of the absolute peak in sources, total number of sources within the cylindrical volume, number of flashes from sources, and the IC:CG ratio. To calculate the number of flashes from sources, we ran the flash grouping algorithm using the selected sources (all sources detected within 10 km of a cell). Refer to Johnson et al. (1998), Witt et al. (1998), and Stumpf et al. (1998) for how the storm cell radar characteristics were calculated.

To obtain a four-dimensional (x, y, z, and t) representation of a storm's radar and lightning structure the following cross-sections of the data were produced on a single plot: time-height, x distance-height, y distance-height, and x-y distance (see Fig. 2). The x distance represents east-west, and the y distance represents north-south in the plots. LDAR II source density was computed at 1 km resolution, except for the time-height panels, which were constructed using 5 s time and 1 km height resolutions. For the vertical cross sections, the number of sources was summed in each 1 km^2 grid box (x-height, y-height) over the depth of the cuboids (60 km; we plotted data within a 60 km by 60 km horizontal box centered on the cell). The horizontal cross section source density was computed using a 1 km^2 (x-y grid box) by 20 km height cuboid (most lightning was detected within 20 km of sea level).

The radar reflectivity vertical and horizontal cross sections were constructed in a similar method, but the values shown are the mean reflectivity for each cuboid. The mean reflectivity values were conditional in that only points in the cuboids that had reflectivity values above 0 dBZ were used. For the horizontal cross

sections only values above the freezing level were used to calculate the mean reflectivity. This was done to test the idea that lightning production is highly dependent on the existence of hydrometeors above the freezing level in a thunderstorm.

The total lightning (LDAR II) and radar history following a storm cell will be shown in a time-height display (Fig. 7). For each radar volume scan, the mean reflectivity of a storm was calculated for each height at 0.5 km intervals. Only values within 20 km in horizontal distance of the storm cell location, determined from WDSS-II, were used to calculate the mean reflectivity at each height for each volume scan. Contours of the total number of LDAR II sources in each 1 km height interval within 20 km horizontal distance of the storm cell for each radar volume scan interval were overlaid on the radar data. A volume scan interval for this data is approximately 5 minutes.

3. TOTAL LIGHTNING AND RADAR OBSERVATIONS OF SUPERCELLS

3.1 *Lightning and Radar Reflectivity Overlays*

Figure 2 shows cross sections of the total lightning source density and mean reflectivity of a supercell on 13 October 2001. The LDAR II and WSR-88D data shown are from the time period 001537 to 002034 UTC. The height of maximum lightning activity remains constant near 10 km during the 5 minute period shown. The plan view radar structure shows tight reflectivity gradients, especially on the southwest side of the supercell, and the shape of the 55 dBZ contour (which encompasses the hail report) is indicative of a hook, two classic signatures of a mature supercell. The reflectivity contours tilt downwind (00 UTC proximity sounding at FWD indicates southwest winds of 30 knots at 700 hPa) with height in the east-west vertical cross section. Note values greater than 40 dBZ extend upwards of 10 km MSL (above the -40°C isotherm). Both vertical cross sections indicate reflectivity maxima (55 dBZ) aloft above the hail report. The hail report in the height-y cross section is within a weak echo reflectivity region.

The greatest LDAR II source density in all cross sections is within areas of reflectivity gradient. The areas of maximum lightning activity in the vertical cross sections are located above where the reflectivity core extends upward at x, y position (-64, 55). The strongest updraft (determined by the greatest vertical extent of reflectivity) is at this location, and is ideal for charge separation and lightning. The peak in lightning sources and flash origins are at 10 km and 11 km MSL, respectively. 3846 sources comprising 220 flashes are included in this plot (an average of 17 sources per flash).

A very interesting observation in the plan view is the lack of lightning activity in the rear part of the storm (southwest side). Note the absence of any activity near the hail report, where the mean reflectivity is over 55 dBZ! The majority of lightning activity occurred most likely between the main updraft and the forward flank downdraft of the supercell (see Lemon and Doswell (1979) for locations of vertical drafts in a supercell).

This supercell produced an F2 tornado (*Storm Data* 2001) between 010010 and 010507 UTC (Fig. 3). There is more lightning activity at lower-levels than 40 minutes earlier (Fig. 2), indicating the storm possibly has weakened. This also could be due to the storm being 30 km closer to the center of the LDAR II network (range effects on the LDAR II data will be discussed later). However, the reflectivity structure of the supercell shows that it has weakened as well. The reflectivity does not extend upward as high as earlier; the 40 dBZ contour in the vertical cross sections only extends to about 7 km MSL as opposed to being above 10 km in figure 2. Another indication that this is a weaker storm than earlier is that the maximum mean reflectivity (plan view) in the cell is a small area of 50-55 dBZ, while figure 2 shows a larger area of greater than 55 dBZ.

The mean reflectivity tilts downwind once again, and the maximum LDAR II source density is above the reflectivity upward protrusion at x = -17 km in the x-height cross section. The peak number of sources is located at 10 km MSL (above the -40°C isotherm), and there are two peaks in the height histogram of flash origins: 4 km (near the freezing level) and 10 km MSL. There were 9159 sources that comprised 196 flashes in this plot (about 47 sources per flash).

The tornado's path is in the rear flank of the supercell (see plan view of Fig. 3). The tornado was reported to occur throughout this volume scan time, and there are no abrupt changes in the altitude of maximum lightning activity according to the time-height plot. A hook is apparent in the mean reflectivity (observe the 35 dBZ contour at (-25, 72)). The WDSS-II indicated mesocyclone was within the hook region, along with the tornado path. This indicates the mesocyclone detection algorithm (Stumpf et al. 1998) performed quite well. As in figure 2, notice
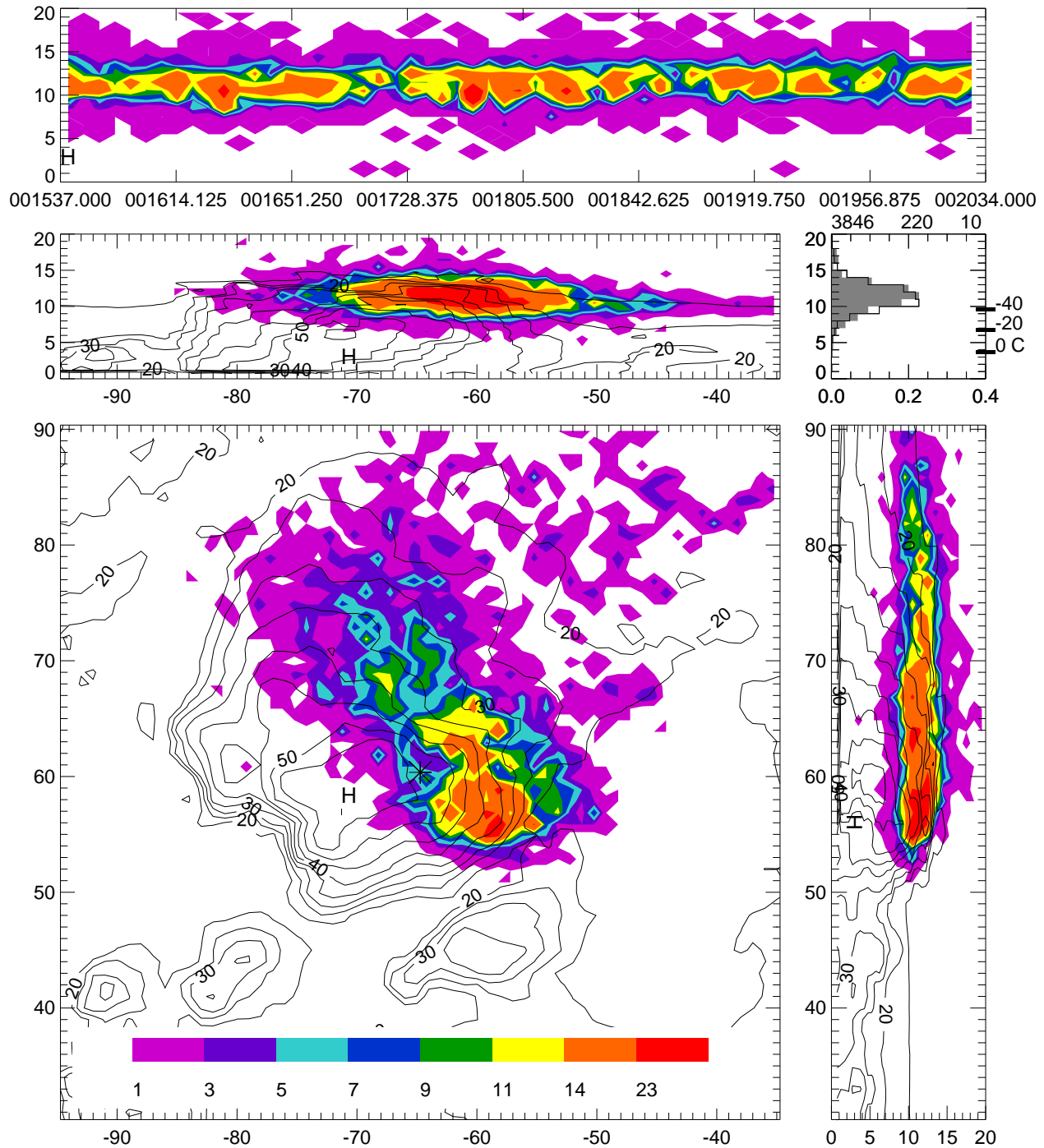
Figure 2. LDAR II source density and mean radar reflectivity of a supercell on 13 October 2001. The uppermost panel shows the time (UTC) versus height display of lightning source density at 0.5 s and 1 km resolutions. The lower left panel shows the plan view cross section of mean reflectivity (dBZ) overlaid on source density (color bar gives values in sources km^{-2}). The resolution of the LDAR II and radar data is 1 km. The asterisk is the location of the radar-detected mesocyclone by WDSS-II. The two panels which flank the horizontal cross section are the vertical cross sections (x-height and height-y) of source density and mean reflectivity. The height resolution of the LDAR II data is 1 km and of the radar data 0.5 km. The color bar is not associated with these panels or the time-height panel. A height histogram of the number of sources and flash origins (shaded) at 1 km intervals is plotted to the right of the x-height cross section. Environmental temperature levels are plotted as bars, and the total number of sources, flashes, and peak source height (km) are given above the histogram. The "H" in the panels represents the time and location of a severe hail report. The axes are labeled as distances (x: east-west, y: north-south) from the KFWS radar (located at 0, 0) and in the vertical are heights in km MSL.
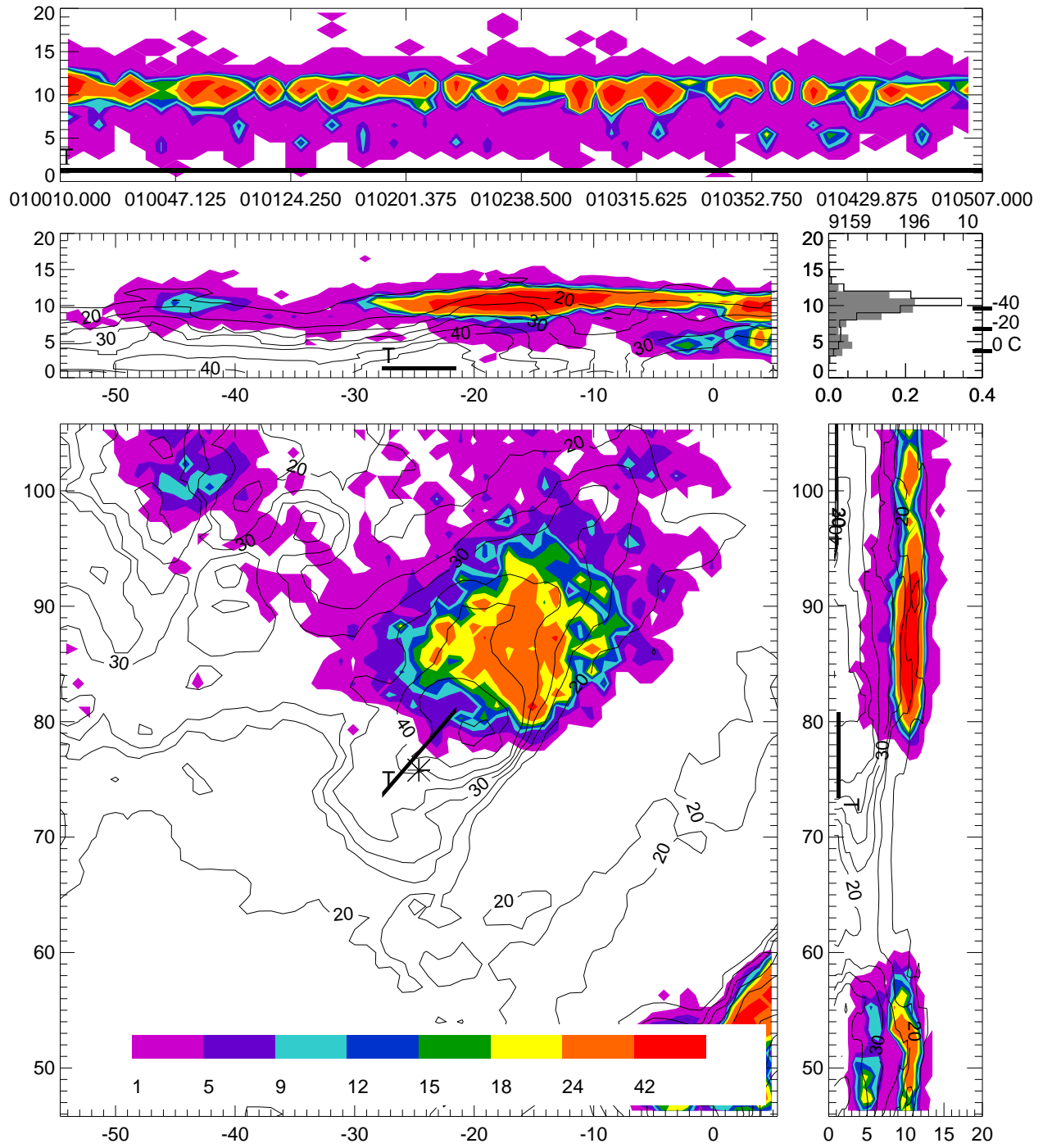
Figure 3. Same as figure 2, except for 010010 to 010507 UTC and "T" gives the location and track of a reported F2 tornado associated with this supercell.

that most of the lightning activity occurred in areas of reflectivity gradient downwind of the storm.

3.2 *Time Series of Radar and Lightning Characteristics*

Several different "lightning heights" were computed to diagnose the intensity of the supercell. As was shown in figures 2 and 3, the areas of maximum lightning activity were above where reflectivity extended upward, representative of a strong updraft. Hence, it is our hypothesis that lightning heights can be used to diagnose storm intensity. These were calculated by finding the 95th percentile (lightning-based storm top), peak, median, and lower quartile height of all LDAR II sources located within 10 km of the radar-defined mesocyclone for each radar volume scan time interval. Figure 4 reaffirms that the storm reached it's peak intensity over 10 minutes prior to the report of the first tornado (F2) touchdown at 005000 UTC (top height 15 km, peak height 12 km, median height 12 km, and lower quartile height 11 km). All heights show significant descent to a minimum during the second tornado (F2) at 010700 UTC. The two severe hail reports (001500 and 014400 UTC) occurred when the storm cell was relatively intense, and this agrees with the storm structure shown in figure 2.
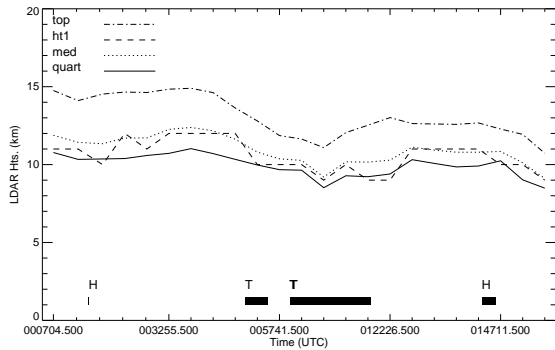

Figure 4. Time history of LDAR II lightning height characteristics for sources within 10 km of the 13 October 2001 mesocyclone: lightning-based storm top (95th percentile: top), peak height (ht1), median height (med), and lower quartile height (quart). The duration of severe hail (H) and tornado (T) events are drawn as bars along the x-axis. Each x-tick mark represents the midpoint of a volume scan.

To test the idea that the storm was weakening during tornadogenesis, we examined the radar-derived storm cell and mesocyclone diagnostics given in WDSS-II. Figures 5 and 6 show that all radar characteristics decrease to a minimum in intensity during the tornadoes. Radar

top (peak height of the 30 dBZ echo of the cell) peaks at 12 km about 5 minutes before the first tornado and decreases to a minimum of 6 km during the middle of the second tornado. The severe hail index (SHI), which is an integration of the reflectivity above the freezing level, reaches a maximum near 001800 UTC, nearly 30 minutes before the first tornado was reported, and decreases to a value near 0 during the second tornado. The VIL and MSI follow a similar trend.
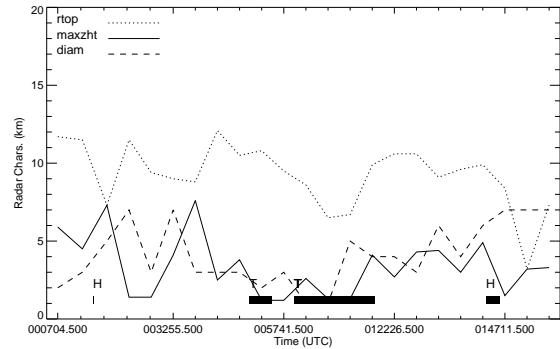

Figure 5. Time history of radar-derived diagnostics for the 13 October 2001 supercell: radar top (rtop), maximum reflectivity height (maxzht), and mesocyclone diameter (diam). The occurrences of severe hail (H) and tornadoes (T) are also shown.
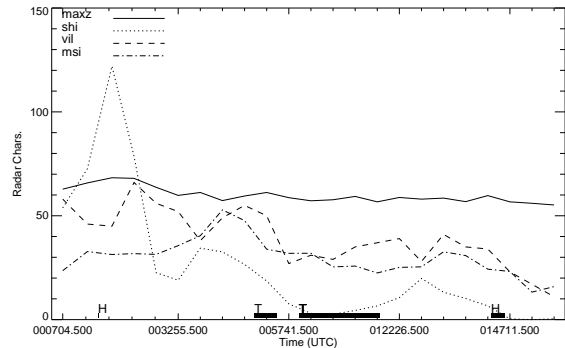

Figure 6. Same as figure 5, but for maximum reflectivity (maxz, dBZ), severe hail index (shi), vertically integrated liquid (vil), and mesocyclone strength index (msi). The shi and msi were scaled to fit on the plot by 5 and 100, respectively.

The significant updraft weakening of the storm during tornadogenesis is apparent in figure 7. The vertical extent of mean reflectivity peaks at 004300 UTC, about 7 minutes or over 1 volume scan before the first tornado touchdown. The height of the 30 dBZ contour is 13 km, and descends to 7 km MSL during the second tornado (010700 UTC). The height of maximum LDAR II source density (denoted by the 800 sources km^{-1} (5 minutes)[-1]) follows the radar contours' descent

and reaches a minimum during the second tornado as well. There is a secondary intensification to the storm's updraft apparent at 012226 UTC, preceding a severe hail report at 014500 UTC. The area of > 55 dBZ reflectivity below 3 km at 012226 UTC is believed to be an analysis error as it has no time continuity. The hail report at 001500 UTC has an elevated reflectivity maximum of 50-55 dBZ at 5 km MSL associated with it that descends to the ground by 002200 UTC.
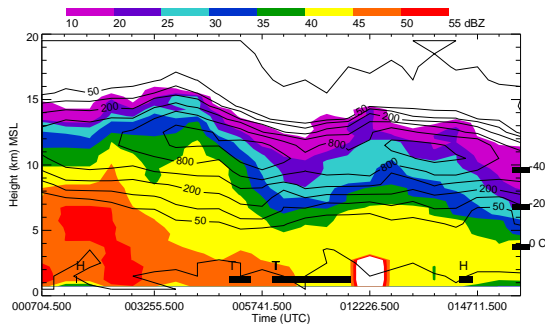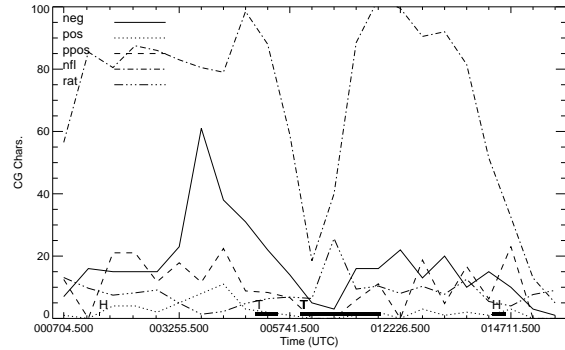

Figure 8. Time history of lightning characteristics calculated within 10 km of the 13 October 2001 mesocyclone for each radar volume scan interval. The –/+ CG flash rate (neg/pos), percent positive CG flashes (ppos), total flash rate (nfl), and IC:CG ratio (rat) are shown. Severe hail (H) and tornado (T) reports are also plotted.

3.3 *Relationships between Lightning and Radar Characteristics*

The previous results indicate that radar reflectivity and lightning storm characteristics are related. This section uses correlation analysis to test the hypothesis that if radar characteristics indicate a storm is becoming more intense, there is a corresponding signal in the lightning characteristics. The support of this hypothesis indicates that lightning can be used to predict storm evolution, an idea that has been tested by many lightning researchers (i.e., MacGorman et al. 1989, Carey and Rutledge 1998, Harlin et al. 2000, Lang and Rutledge 2002, MacGorman et al. 2002). This study is different from the aforementioned ones in that it uses cell characteristics from WDSS-II and uses LDAR II source heights as a measure of storm updraft strength.

Correlations between lightning and radar characteristics calculated for each volume scan during the 13 October 2001 supercell are shown in Table 1. The lightning-based storm top (top) is significantly correlated with the radar measures of storm strength. The VIL-top positive correlation is the highest at 0.82. The number of flashes determined from the source data is also positively correlated with these measures, and its highest r value is with VIL (0.66). The MSI, a measure of the strength of the mesocyclone, is significantly positively correlated with both LDAR II characteristics shown. Hence, the hypothesis that the lightning characteristics used in this study can predict storm strength is supported.

Figure 7. Time-height plot of mean radar reflectivity (see color bar at top) and LDAR II source density (sources km^{-1} (5 minutes)$^{-1}$) for the 13 October 2001 supercell between 000436 and 015437 UTC. To calculate these values, only radar and lightning data were analyzed within 20 km from the storm mesocyclone during each volume time interval. Severe hail (H) and tornado (T) reports and the ambient temperature levels are also shown. See section 2 for more details on the plot construction.

The most intense lightning flash rates of this supercell also occur before the tornado reports (Fig. 8). The total (IC and CG) flash rate peaks at 200 flashes per volume scan (5 minutes) (note the number of flashes was divided by 2 to fit the curve on the plot) at 004800 UTC. The –CG flash rate reaches a maximum value of 60 flashes (5 minutes)$^{-1}$ at 003800 UTC. Both rates decrease by up to a factor of 5 to a minimum during the second F2 tornado (report beginning at 010000 UTC). The IC:CG values are near 10 in the initial stage of the storm, decrease to a minimum the same time the –CG flash rate peaks, reach a maximum value of 25 during the second F2 tornado (the total and CG flash rates are 5 minutes out of phase in their minimum values), and then is steady near 10 throughout the remainder of the period. The percentage of +CG flashes is also at a minimum during the second tornado.

	r^2	r	sig
quart-dist	0.4292	0.6551	*
med-dist	0.4361	0.6604	*
top-dist	0.6262	0.7913	*
ht1-dist	0.2059	0.4537	
totpts-dist	0.0356	-0.1886	
nfl-dist	0.0694	0.2634	
maxz-dist	0.7317	0.8554	*
maxzht-dist	0.1432	0.3784	*
rtop-dist	0.1630	0.4037	*
shi-dist	0.7110	0.8432	*
vil-dist	0.5122	0.7157	
maxz-top	0.4862	0.6973	*
maxz-nfl	0.1680	0.4099	
maxzht-top	0.1921	0.4383	*
maxzht-nfl	0.0181	0.1346	
rtop-top	0.2657	0.5155	*
rtop-nfl	0.3242	0.5694	*
shi-top	0.4703	0.6858	*
shi-nfl	0.1144	0.3382	
vil-top	0.6743	0.8211	*
vil-nfl	0.435	0.6596	*
msi-top	0.3214	0.5669	*
msi-nfl	0.2577	0.5076	*

Table 1. Correlation analysis of lightning and radar characteristics for the 13 October 2001 tornadic supercell. The linear correlation coefficient is given by r, and the correlations that are significant (sig) at the $p=0.05$ level are marked by *. The characteristics shown include: LDAR II lower quartile height (quart), median (med), 95th percentile (top), and peak source density height (ht1), total source points (totpts), number of flashes (nfl), maximum reflectivity (maxz), max. reflectivity height (maxzht), radar top (rtop), SHI, VIL, MSI, and distance from the LDAR network center (dist). The LDAR II characteristics were calculated using data within 10 km of the mesocyclone.

3.4 *Non-tornadic Supercell*

To observe if the above signatures associated with the 13 October 2001 tornadic supercell may have been unique to a tornadic storm, radar and lightning data were analyzed from a non-tornadic supercell from the same event (from 005015 to 015437 UTC). The lightning heights show a general upward trend during this period (Fig. 9). The 95th percentile height is 12.5 km at 005244 UTC, and reaches a maximum value at 014200 UTC of 14.5 km.
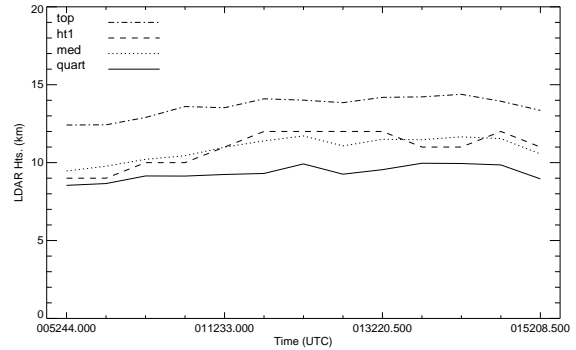

Figure 9. Same as figure 4, but for a non-tornadic supercell on 13 October 2001. There were no severe storm reports associated with this storm.

The mean reflectivity history of the non-tornadic supercell shows an increase in the vertical extent of the storm to a maximum at 013220 UTC (Fig. 10). The maximum height of the 30 dBZ contour increases from 10 km at 010200 UTC to over 14 km at 013220 UTC. There is a corresponding increase in height of the maximum LDAR II source density (3200 sources km^{-1} (5 minutes)$^{-1}$), but the trend is not as drastic as with the tornadic storm shown in figure 7 (this observation agrees with the trends shown in figures 4 and 9).
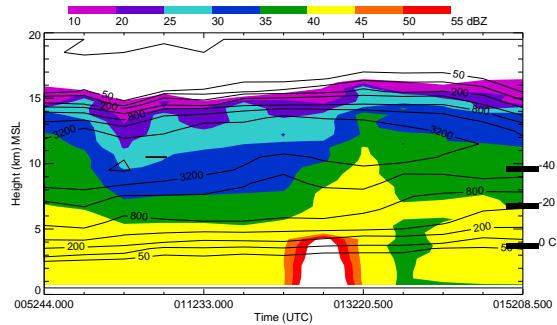

Figure 10. Same as figure 7, except for a non-tornadic supercell on 13 October 2001 between 005015 and 015437 UTC. The area of > 55 dBZ below 5 km at 012700 UTC is an analysis error.

Surprisingly, the maximum source density shown in figure 10 (6400 sources km^{-1} (5 minutes)$^{-1}$) occurs at 010200 UTC when the radar reflectivity contours are at lower altitudes (indicative of weaker updraft than at 013220 UTC). Comparing figures 7 and 10 shows that the maximum contoured source densities are greater for the non-tornadic supercell (6400 vs. 1600 sources). We believe this is because the non-tornadic storm traversed closer to the LDAR II network than the tornadic supercell (mean

distance from the network throughout each storm's lifetime = 71 km for the tornadic storm, 39 km for the non-tornadic storm).

3.5 *Bimodal Source Density Height Distributions*

Most analyzed time intervals show a unimodal height distribution of LDAR II sources (see Fig. 2). Figure 11 shows an example of a supercell (different from previous supercells shown) with a bimodal distribution in LDAR II sources. The time-height and vertical cross sections show two horizontally expansive layers connected by a vertical bridge of large values of lightning source density for the cell located at (40, 60). The upper layer (12 km MSL) has greater horizontal extent than the lower layer. The x-height cross section includes lightning from more than one storm (see cell with lightning hook at (50, 47)). The cell at (50, 47) is at an earlier stage of development according to radar reflectivity data (not shown) than the cell at (40, 60). Note how this cell does not have a well developed lower layer of lightning activity – possibly a signature of a storm at an initial stage of development.

The height histogram in figure 11 indicates two levels of maximum lightning activity at 4 and 12 km MSL. The peak at 12 km occurs at an environmental temperature of well-below -40°C, while the lower one is slightly above the freezing level. VHF TOA lightning detection systems like LDAR II detect more sources from positive charge regions than negative charge regions because negative polarity breakdown into positive charge regions is noisier at radio frequencies (RF) than positive breakdown into negative charge regions (Shao and Krehbiel 1996). The distribution of sources in figure 11 reveals maxima where positive charge regions are typically observed by more direct means (electric field soundings) (Stolzenburg et al. 1998) and agree with charge separation theories based on temperature and liquid water content (Saunders 1993) (we assume higher liquid water content at lower levels near 0°C in the storm).

Three maxima of flash origins (gray shaded) are located at 4 km, 9 km, and 12 km MSL in the histogram. The lower-level and upper-level peaks of flash origins represent where the CG and IC flashes most likely initiated, respectively (the 9 km level is probably associated with normal polarity IC flashes also). Negative CG flash density values are greater than 0.22 flashes km^{-2} in two areas of the supercell. These maxima in CG flash density are not well-associated with maxima in LDAR II source density (they flank the concentration of source density maxima of > 88 sources km^{-2} near (35, 60)). Note that the developing storm at (50, 47), which does not have a well-developed lower charge region, has lower –CG flash density values (near 0.02 flashes km^{-2}) than the mature storm at (40, 60). A lower positive charge region may be required for –CG flashes (Mansell et al. 2002).

The cells examined that exhibited a distinct multimodal height distribution of LDAR II sources occurred close to the network center (within 50 km). However, there were several mature storms analyzed within 50 km of the network that did not exhibit multimodal characteristics. This behavior was observed in other case studies (non-supercells on other dates) as well. There is speculation that the lower positive charge region of a thunderstorm is more detectable by the LDAR II system for closer storms (Carey 2004, personal communication). The reasoning for this speculation is unclear and will be studied further.

4. DISCUSSION AND CONCLUSIONS

The horizontal cross sections in figures 2 and 3 show that most lightning occurs in areas of radar reflectivity gradient. Rust et al. (1982) and Proctor (1991) found lightning origins at the edges of high radar reflectivity precipitation cores, where reflectivity and vertical velocity horizontal gradients were large. Greatest charge separation occurs where there are gradients in vertical velocity and gradients in radar reflectivity may be used as a proxy for vertical velocity gradients. Hence, lightning activity is greater where gradients in reflectivity occur, and our observations support this hypothesis.

The maximum LDAR II source density in the vertical cross sections of figures 2 and 3 is located in reflectivity gradient above where the reflectivity contours extend upwards. These areas are indicative of strong updrafts that increase charge separation processes and elevate precipitation particles and their associated charge.

There are no lightning holes apparent in our analysis surrounding the tornado or its parent mesocyclone as discussed by McCaul et al. (2002) and Wiens et al. (2002). Figure 3 shows a lightning hook at (-22, 78) and that most lightning is downshear of the mesocyclone (Fig. 2 also shows this). Ray et al. (1987) also show that lightning tended to be downshear of the main updraft and reflectivity core in a supercell. Charge is clearly being advected on the precipitation
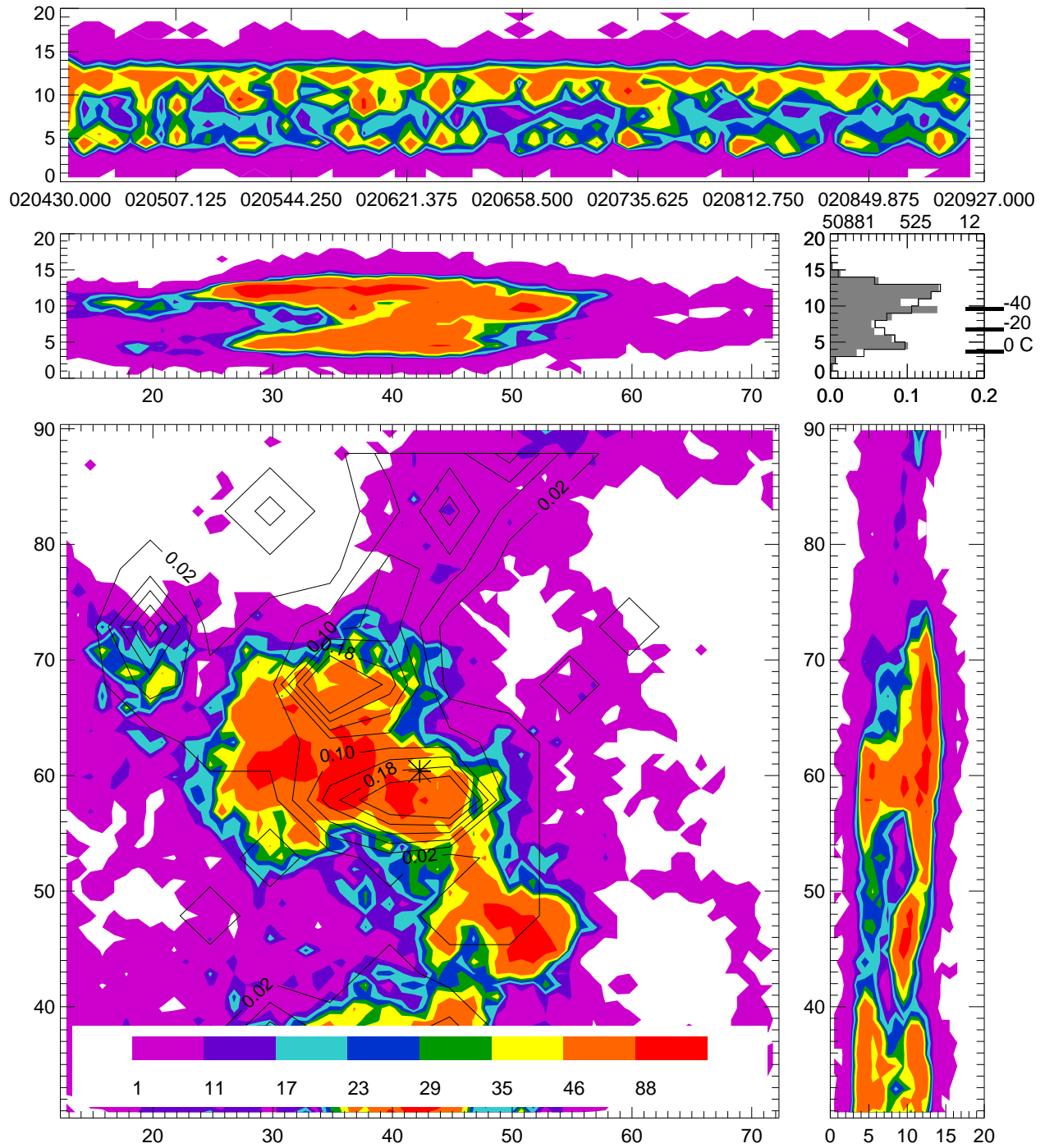
Figure 11. Same as figure 2, except for 020430 to 020927 UTC and instead of mean radar reflectivity, negative CG flash density is overlaid on the LDAR II source density in the plan view. The resolution of the CG data is 5 km.

particles when there is significant wind shear (as is the case typically with supercell environments).

The peaks in the height histograms of LDAR II sources (Figs. 2, 3, 11), which we hypothesize to be the locations of positive charge regions, are located at environmental temperatures below -40°C and just above the freezing level (when a second peak exists as in Fig. 11). At these temperatures and likely liquid water contents (high LWC near the freezing level, zero LWC (all ice) at T < -40°C), Saunders (1993) indicates positive charging of precipitation particles. Figures 2, 3, and 11 also show that the distribution of flash origins peak on the edges of source peaks (especially note the peak at 9 km MSL of flash origins in Fig. 11). Electric fields are at maximum values *between* oppositely charged regions. Lightning is initiated where the electric field is the strongest (MacGorman and Rust 1998, p. 203). If we assume that a negative charge region is located at the minimum in the source height distribution, our observations support the hypothesis that the source peaks represent positive charge regions as the maximum number of flash origins is located between oppositely charged regions. However, figure 11 shows that the highest and lowest flash origin peaks are also where the source peaks are located, contrary to the hypothesis.

The lightning heights (lower quartile, median, 95th percentile, and peak heights) calculated with the LDAR II data are useful indicators of storm updraft strength. Figures 4, 5, and 6 show that when radar storm cell characteristics, such as the radar top, SHI, and VIL, indicate a stronger storm, the lightning heights are higher. The radar top has two maxima at 004300 UTC and 012227 UTC, near the same times as when the lightning heights are at their highest. As a storm's updraft intensifies, precipitation particles are lofted higher, especially the lighter ice crystals that are typically charged positively (Saunders 1993). Hence, the radar top and LDAR II sources, which show where positive charge is in the storm, are at higher altitudes. Stolzenburg et al. (1998) show by more direct means (electric field balloons) that charge regions are higher in altitude when the balloon ascent rate (a proxy for updraft strength) is larger.

Table 1 also supports the hypothesis that the lightning characteristics calculated in this study can be used as indicators of changes in storm intensity. Maximum reflectivity, maximum reflectivity height, radar top, SHI, VIL, and MSI all show significant positive correlations with the lightning parameters shown (95th percentile height

and total number of flashes) for the tornadic supercell. These results agree with those of Mazur et al. (1986), who show a storm's maximum flash rate (mostly composed of IC flashes) typically occurs when the storm height has peaked. The advantages of the characteristics calculated from LDAR II data are that the time and spatial resolution of the lightning data are better than WSR-88D data (these characteristics can be calculated for every minute or less of the storm's lifetime as opposed to the 5-6 minutes required for a radar volume scan).

The lightning and radar characteristics shown in figures 4-8 show a significant weakening in the supercell prior to and during the reported tornado touchdowns. Lightning heights show significant descent and radar characteristics like the SHI peak well-before the tornado touchdowns. Most of these indicators have their absolute minimum values during the second tornado, rated F2. Figure 7 clearly shows the storm is going through a collapse phase during tornadogenesis. Both –CG and total flash rates decreased by at least a factor of 5 to a minimum during the F2 tornado (Fig. 8). Comparing the plan views of figures 2 and 3, the WDSS-II indicated mesocyclone becomes more separated from the total lightning activity during the tornadic stage of the storm. This may explain why the flash rates decreased substantially as we only chose lightning data within 10 km of the mesocyclone to calculate the characteristics. However, we conducted a similar analysis as shown in figure 8 using data within 20 km of the mesocyclone and found similar results. Recent studies show the rate of VHF emissions tended to increase at middle levels of a storm prior to tornado occurrence (MacGorman et al. 2002). Tornadoes tended to occur during or shortly *after* updraft surges inferred from lightning.

Lemon and Doswell (1979) explain that tornado touchdown occurs when the updraft of an intense supercell weakens in magnitude and extent and the downdraft (rear flank) of the storm intensifies. The mesocyclone becomes divided between updraft and downdraft. This theory is supported by our observations: all lightning and radar characteristics indicate the storm is indeed weaker (updraft less intense and/or downdraft overtaking the storm) while the tornadoes are on the ground. Caution must be taken in that there can be errors in the timing and location of the reported tornado. Another tornadic supercell, from the same event, is being analyzed. Early results show the same behavior (radar and lightning characteristics decrease to minimum values during tornadogenesis) as the tornadic supercell

discussed here. The non-tornadic supercell examined in this study shows a gradual increase in lightning heights throughout the storm's lifetime. The lightning and radar trends shown for the tornadic storm are more abrupt and appear to be related to tornadogenesis.

A comparison of figures 4 and 8 shows that the lightning heights, total flash rate, and –CG flash rate are at maximum values at similar times (003800 UTC). The IC:CG ratio is at a minimum at this time (less than 5). The lightning heights in this study have been shown to be indicators of storm updraft intensity. MacGorman et al. (1989) suggest that as a storm's updraft intensifies, IC flash rate increases and CG flash rate decreases as oppositely charged regions are brought closer to each other higher in the storm producing higher electric fields there. Thus, our observation that total flash rate increases with updraft strength as indicated by the lightning heights appears to support this hypothesis. A maximum –CG flash rate at 003800 UTC, however, does not support the elevated charge region hypothesis proposed by MacGorman et al. As discussed earlier, the charge regions detected by the LDAR II instrument are most likely positively charged, and the MacGorman et al. hypothesis claims the negative charge region is lifted in a stronger updraft. The modeling study by Ziegler and MacGorman (1994) shows that in a strong supercellular updraft, *both* the main negative and positive charge regions are elevated (see their Fig. 7). Hence, we assume an elevated positive charge region, as detected by the LDAR II system, indicates an elevated negative charge region.

As the distance between the storms and LDAR II network center increases, certain range effects are apparent. When the tornadic supercell is closer to the network in figure 3 (65 km from the network compared to 94 km for the storm in Fig. 2), more lightning is detected at lower levels. The maximum values of source density are larger in the closer storm in figure 10 (6400 sources km^{-1} (5 minutes)$^{-1}$) compared to figure 7 (1600 sources km^{-1} (5 minutes)$^{-1}$). This may be attributable to the storm in figure 10 being more intense than the storm shown in figure 7, but the radar characteristics indicate the storm with the lower maximum source density to be more intense (larger values and heights of maximum reflectivity). There are also more sources per flash in the closer storm (47 sources per flash) shown in figure 3 compared to the more distant storm (17 sources per flash) shown in figure 2. The flashes could be longer in the closer storm, but we analyzed many storms at different distances from the network and found the same relationship. Hence, significantly more sources are detected in closer storms. Figure C3 in Carey et al. (2004) shows a rapid decrease in lightning source detection efficiency of the DFW LDAR II with range. The source density can not be used as an indicator of storm strength when comparing storms from different distances from the network.

Determining the number of flashes from the LDAR II source data mitigates the decrease in source detection efficiency with range. The correlation between total points detected within 10 km of the tornadic mesocyclone and the mesocyclone's distance from the network is -0.19 (Table 1). Correlations we've calculated between these two variables for several other storms have been negative as well, and the majority of the correlations have been more significant than the correlation shown for this particular supercell. The correlation between total number of flashes and distance is 0.26, showing that the number of flashes increases the further the storm is from the network (between 57 and 101 km). This indicates the storm is more intense when it is farther away from the network. The correlations between radar characteristics and distance agree with this interpretation (i.e., SHI-distance correlation is significant with a value of 0.84). The increase in the number of flashes with distance may include an instrument/algorithm effect: a lower number of sources are detected with increasing range from the network and this may have a tendency to segregate sources from one flash into several flashes because the space and time criteria of the flash grouping algorithm are not met.

Boccippio et al. (2000) have shown that an altitude error exists with LDAR data. Using a large database from the KSC network, their figure 7 shows a systematic increase in the altitude of maximum source density with increasing range from the network (especially at ranges greater than 150 km). They show this error is due to increasing radial location errors with distance from the network. Thomas et al. (2004) claim that "uncertainty in the elevation angle is the dominant factor in the source height values." The supercell in figure 4 steadily moves toward the LDAR II network center from 000436 (101 km range) to 015437 UTC (57 km range). The heights in figure 4 show descent until 010800 UTC, but then increase to a relative maximum height at 012227 UTC. The altitude error is not significant enough to mask the trends associated with the storm's intensity variations. This agrees with Boccippio et al.'s figure 7, which shows that large altitude errors (greater than 2 km) do not occur within 150 km

from the network. It is our recommendation to not use lightning height information as an indicator of storm intensity beyond 150 km from the network. All lightning heights show a strong positive correlation with distance in Table 1, which may be a result of the systematic altitude error discussed in Boccippio et al. However, the supercell's radar characteristics are also positively correlated with distance from the network, indicating that the storm is most intense when at a greater range from the network. Hence, the lightning heights shown here are useful indicators of storm updraft intensity (especially because of the observations mentioned above about the inability of systematic altitude errors to mask true storm intensity).

Total lightning data has been shown to be quite useful in diagnosing supercell intensity. Used in conjunction with radar data, researchers and forecasters will have a better understanding of thunderstorm morphology and its relation to the occurrence of severe weather (tornado, large hail) at the ground. The advantages of volumetric LDAR II data include higher temporal and spatial resolutions compared to WSR-88D data. LDAR II data is useful for these purposes within 150 km from the network; beyond this distance range and altitude errors are significant. LDAR II source density is not very useful to compare storms at different ranges as the number of detected sources decreases rapidly with distance from the network.

5. REFERENCES

Boccippio, D. J., S. Heckman, S. J. Goodman, 2000: A diagnostic analysis of the Kennedy Space Center LDAR network: 1. Data characteristics. *J. Geophys. Res.*, **106** (D5), 4769-4786.

Carey, L. D., and S. A. Rutledge, 1998: Electrical and multiparameter radar observations of a severe hailstorm. *J. Geophys. Res.*, **103**, 13979-14000.

Carey, L. D., M. J. Murphy, T. L. McCormick, and N. W. S. Demetriades, 2004: Lightning location relative to storm structure in a leading-line, trailing-stratiform mesoscale convective system. *J. Geophys. Res.*, in press.

Cummins, K. L., M. J. Murphy, E. A. Bardo, W. L. Hiscox, R. B. Pyle, and A. E. Pifer, 1998: A combined TOA/MDF technology upgrade of the U. S. National Lightning Detection Network. *J. Geophys. Res.*, **103**, 9035-9044.

Cummins, K. L., M. J. Murphy, and J. V. Tuel, 2000: Lightning detection methods and meteorological applications. Preprints, *4th International Symposium on Military Meteorology*, Malbork, Poland, 85-100.

Demetriades, N., M. J. Murphy, and K. L. Cummins, 2001: Cloud and cloud-to-ground lightning detection at LF and VHF: Early results from Global Atmospherics Dallas-Fort Worth LDAR II and IMPACT/ESP research networks. *Eos Trans. AGU*, **82**, Fall Meet. Suppl., Abstract AE21A-07.

Harlin, J. D., T. D. Hamlin, P. R. Krehbiel, R. J. Thomas, W. Rison, and D. Shown, 2000: LMA observations of tornadic storms during STEPS 2000. *Eos Trans. AGU*, **81**, Fall Meet. Suppl., Abstract A52C-25.

Hondl, K. D., 2003: Capabilities and components of the Warning Decision Support System - Integrated Information (WDSS-II). Preprints, *19th Conf. On Interactive Info. Processing Systems*, Long Beach, CA, Amer. Meteor. Soc., CD preprints.

Johnson, J. T., P. L. MacKeen, A. Witt, E. D. Mitchell, G. J. Stumpf, M. D. Eilts, and K. W. Thomas, 1998: The storm cell identification and tracking algorithm: An enhanced WSR-88D algorithm. *Wea. Forecasting*, **13**, 263-276.

Lang, T. J., and S. A. Rutledge, 2002: Relationships between convective storm kinematics, precipitation, and lightning. *Mon. Wea. Rev.*, **130**, 2492-2506.

Lemon, L. R., and C. A. Doswell III, 1979: Severe thunderstorm evolution and mesocyclone structure as related to tornadogenesis. *Mon. Wea. Rev.*, **107**, 1184-1197.

MacGorman, D. R., and K. E. Nielsen, 1991: Cloud-to-ground lightning in a tornadic storm on 8 May 1986. *Mon. Wea. Rev.*, **119**, 1557-1574.

MacGorman, D. R., and W. D. Rust, 1998: *The Electrical Nature of Storms*. Oxford University Press, 422 pp.

MacGorman, D. R., A. A. Few, and T. L. Leer, 1981: Layered lightning activity. *J. Geophys. Res.*, **86**, 9900-9010.

MacGorman, D. R., D. W. Burgess, V. Mazur, W. D. Rust, W. L. Taylor, and B. C. Johnson, 1989: Lightning rates relative to tornadic storm evolution on 22 May 1981. *J. Atmos. Sci.*, **46**, 221-250.

MacGorman, D., D. Rust, O. van der Velde, M. Askelson, P. Krehbiel, R. Thomas, B. Rison, T. Hamlin, and J. Harlin, 2002: Lightning relative to precipitation and tornadoes in a supercell storm during MEAPRS. Preprints, *21st Severe Local Storms Conf.*, San Antonio, TX, Amer. Meteor. Soc., 423-426.

Mansell, E. R., D. R. MacGorman, C. L. Ziegler, and J. M. Straka, 2002: Simulated three-dimensional branched

lightning in a numerical thunderstorm model. *J. Geophys. Res.*, **107**, doi: 10.1029/2000JD000244.

Mazur, V., W. D. Rust, and J. C. Gerlach, 1986: Evolution of lightning flash density and reflectivity structure in a multicell thunderstorm. *J. Geophys. Res.*, **91**, 8690-8700.

Mazur, V., E. Williams, R. Boldi, L. Maier, and D. E. Proctor, 1997: Initial comparison of lightning mapping with operational time-of-arrival and interferometric systems. *J. Geophys. Res.*, **102**, 11071-11085.

McCaul, E. W., J. Bailey, S. J. Goodman, R. Blakeslee, J. Hall, D. E. Buechler, and T. Bradshaw, 2002: Preliminary results from the North Alabama lightning mapping array. Preprints, *21st Severe Local Storms Conf.*, San Antonio, TX, Amer. Meteor. Soc., 427-430.

Orville, R. E., and G. R. Huffines, 1999: Lightning ground flash measurements over the contiguous United States: 1995-1997. *Mon. Wea. Rev.*, **127**, 2693-2703.

Oye, D., and M. Case, 1995: *REORDER: A program for gridding radar data. Installation and use manual for the UNIX version*, NCAR Atmospheric Technology Division, Boulder, CO, 19 pp.

Proctor, D. E., 1971: A hyperbolic system for obtaining VHF radio pictures of lightning. *J. Geophys. Res.*, **76**, 1478-1489.

Proctor, D. E., 1991: Regions where lightning flashes began. *J. Geophys. Res.*, **96**, 5099-5112.

Ray, P. S., D. R. MacGorman, W. D. Rust, W. L. Taylor, and L. W. Rasmussen, 1987: Lightning location relative to storm structure in a supercell storm and a multicell storm. *J. Geophys. Res.*, **92**, 5713-5724.

Rust, W. D., W. L. Taylor, and D. MacGorman, 1982: Preliminary study of lightning location relative to storm structure. *AIAA Journal*, **20**, 404-409.

Shao, X. M., and P. R. Krehbiel, 1996: The spatial and temporal development of intracloud lightning. *J. Geophys. Res.*, **101**, 26641-26668.

Stolzenburg, M., W. D. Rust, and T. C. Marshall, 1998: Electrical structure in thunderstorm convective regions, 3. Synthesis. *J. Geophys. Res.*, **103**, 14097-14108.

Storm Data, 2001: Storm Data and unusual weather phenomena. National Oceanic Atmospheric Administration, National Climatic Data Center, Asheville, NC.

Stumpf, G. J., A. Witt, E. D. Mitchell, P. L. Spencer, J. T. Johnson, M. D. Eilts, K. W. Thomas, and D. W. Burgess, 1998: The National Severe Storms Laboratory Mesocyclone Detection Algorithm for the WSR-88D. *Wea. Forecasting*, **13**, 304-326.

Thomas, R. J., P. R. Krehbiel, W. Rison, S. J. Hunyady, W. P. Winn, T. Hamlin, and J. Harlin, 2004: Accuracy of the lightning mapping array. *J. Geophys. Res.*, **109**, doi: 10.1029/2004JD004549.

Wiens, K. C., S. A. Tessendorf, and S. A. Rutledge, 2002: June 29, 2000 STEPS supercell storm: Relationships between kinematics, microphysics, and lightning. Preprints, *21st Severe Local Storms Conf.*, San Antonio, TX, Amer. Meteor. Soc., 315-318.

Williams, E. R., C. M. Cooke, and K. A. Wright, 1985: Electrical discharge propagation in and around space charge clouds. *J. Geophys. Res.*, **90**, 6059-6070.

Witt, A., M. D. Eilts, G. J. Stumpf, J. T. Johnson, E. D. Mitchell, and K. W. Thomas, 1998: An enhanced hail detection algorithm for the WSR-88D. *Wea. Forecasting*, **13**, 286-303.

Ziegler, C. L., and D. R. MacGorman, 1994: Observed lightning morphology relative to modeled space charge and electric field distributions in a tornadic storm. *J. Atmos. Sci.*, **51**, 833-851.